

A Comprehensive Liquid Simulation Study of Neat Formic Acid

Péter Mináry,[†] Pál Jedlovszky,^{‡,§} Mihaly Mezei,[‡] and László Turi^{*,†}

Department of Physical Chemistry, Eötvös Loránd University, Budapest 112, P.O.Box 32, Hungary, H-1518, and Department of Physiology and Biophysics, Mount Sinai School of Medicine, New York, New York 10029

Received: January 14, 2000; In Final Form: June 21, 2000

An extensive liquid simulation study combining Monte Carlo and molecular dynamics techniques was performed for liquid formic acid. We investigated thermodynamic, dynamic, and spectroscopic properties of the liquid. The examination of several dynamic properties leads to a detailed picture of the molecular contributions to the macroscopic properties of the liquid phase. Although the present model overestimates the diffusion constant by about 25%, the calculated spectral densities for the translational and rotational modes of the solvent in combination with ab initio calculated harmonic frequencies provide a valuable tool in the qualitative assignment of several important features of the low-frequency liquid phase Raman spectrum. The relaxation time scales also give reasonably good agreement with dielectric relaxation and NMR measurements. Hydrogen-bonding dynamics provide interesting additional information on the dynamical time scales. The average lifetime of the strongest types of hydrogen bonds is less than 0.5 ps. The relative population of the dimers with *two* hydrogen bonds undergoes a significant change relative to the gas phase population, the weight of the less stable dimers increasing substantially. Approximately 1% of the molecules participate in hydrogen-bonding patterns which dominate the crystalline phase of the formic acid. As an extension of the present work for the liquid phase, we have also performed calculations for the vapor–liquid equilibrium coexistence curve predicting the critical temperature with 5% error. The application of the thermodynamic integration method results in thermodynamic excess quantities as the excess free energy, entropy, and chemical potential.

Introduction

Understanding the nature of the hydrogen-bonding interactions is a challenge of central importance in wide areas of theoretical and experimental chemistry. The first step in this process involves investigations of small, model molecules. Formic acid, as the simplest carboxylic acid, can be considered such a molecule. Besides its simplicity, formic acid possesses many interesting properties. Regarding the intermolecular interactions, the formic acid molecule with its two oxygen atoms has two hydrogen bond acceptor sites, while the hydroxyl hydrogen and the formyl hydrogen provide two hydrogen bond donor possibilities. The donor characteristics of the formyl hydrogen can appear in unconventional C–H···O type hydrogen bonds.¹ The rich hydrogen-bonding potential leads to a complex dimer potential energy surface with a variety of stable hydrogen-bonded dimers.² The complexity of the hydrogen-bonding patterns is manifest in the condensed phase structures of formic acid. While formic acid forms a well-known cyclic dimer in the gas phase,³ infinite hydrogen-bonding chains with one O–H···O and one C–H···O bonds between the monomeric units dominate the crystalline phase.⁴ The structure of the liquid formic acid is, however, still the subject of intense investigations. The most powerful experimental methods for the structural problem, the X-ray and neutron scattering techniques, predict the presence of open-chain structures.^{5,6} A series of important

properties, such as thermodynamic, dynamic, and electric properties, also reflect the hydrogen-bonding structure and the dynamics of the liquid phase. Many of these properties have been measured on numerous occasions in the past.^{7–14} Reproducing these properties constitutes an important test for the applicability of any theoretical approach for the description of the condensed phases of formic acid.

To explore the connection between the microscopic (atomic) level and the macroscopically observable quantities, one clearly needs a molecular description of the investigated system. Theoretically, liquid simulation techniques furnish the most viable route to gaining insight into the molecular details underlying the structure, the dynamic and other physicochemical properties of the liquid phase. Despite the broad literature of the computer simulation methodology,¹⁵ the number of simulation studies on pure liquid formic acid is surprisingly limited.^{16–18} The purpose of the present paper is to fill this gap and perform a detailed simulation study of neat liquid formic acid. This work represents the final part of a series of investigations beginning with an ab initio study for exploring the formic acid dimer potential surface in which seven stable minima were located.² Next, a new five-site pair potential was developed for formic acid by a numerical parameter fitting procedure to the ab initio dimer potential.¹⁷ A Monte Carlo (MC) simulation study followed, examining the thermodynamic and structural properties of the liquid phase.¹⁸ The performance of the new pair potential is satisfactory; the computed structural and thermodynamic attributes nicely reproduced the corresponding experimental results. Furthermore, the population of the cyclic, C_{2h} dimer with two O–H···O hydrogen bonds has been found relatively small in the neat liquid. As another important

* Corresponding author. E-mail: turi@para.chem.elte.hu. Fax: (36)-1-209-0602.

[†] Eötvös Loránd University.

[‡] Mount Sinai School of Medicine.

[§] On leave from Central Research Institute for Chemistry of the Hungarian Academy of Sciences, Budapest, Hungary.

TABLE 1: Optimized Lennard-Jones Parameters and Charges for the *cis*-Formic Acid Monomer

<i>i</i>	<i>q_i</i> (e)	σ_{ii} (Å)	ϵ_{ii} (kJ/mol)
C	0.44469	3.727	0.376
(C=)O	-0.43236	2.674	1.214
(C-)O	-0.55296	3.180	0.392
(C-)H	0.10732	0.800	0.020
(O-)H	0.43331	0.994	0.100

result, the role of C—H \cdots O interactions has been illustrated in the liquid phase. The liquid structure is described as a two-level hydrogen-bonding network consisting of small, often branching oligomers mainly with O—H \cdots O bonds. The smaller clusters are connected to each other by weaker C—H \cdots O interactions, thus forming a space-filling network of hydrogen bonds.¹⁸

In the present work we consider various further aspects of neat liquid formic acid with emphasis on the dynamic properties as computed from molecular dynamics (MD). We first attempt to qualitatively assign the low-frequency translational and rotational spectra of liquid formic acid. Microscopic details of the relaxation phenomena in solvation processes and NMR spectroscopy are also taken under inspection. The MD methodology makes it possible for us to examine the hydrogen-bonding dynamics. Consequences and possible implications of the hydrogen bond dynamics for the gas and solid phases are considered. We also extend our investigations from the pure liquid phase toward vapor–liquid equilibrium by calculating excess free energies and critical constants (temperature, density). The computed thermodynamic quantities can further verify the applicability of the applied model.

Methods

Classical liquid simulations have been performed on pure formic acid in the present work. We mention at the outset that although the techniques for treating liquid dynamics on ab initio principles have been available for more than 15 years,¹⁹ the size of the present system still requires the classical simulation methodology. Our simulations include microcanonical ensemble molecular dynamics simulations, canonical ensemble MC simulations, and the application of the Gibbs ensemble Monte Carlo method²⁰ with cavity biased particle insertion.²¹ The computational details will be given directly before the sections outlining the actual results. In this part of the paper we collect the common features of the simulation techniques employed.

In the simulations we applied the cubic simulation box and standard periodic boundary conditions with the minimum image convention. For describing the interactions between the formic acid molecules we employed the five-site potential developed earlier.¹⁷ The potential consists of the sum of electrostatic and Lennard-Jones type interactions. At this point we find it necessary to note that due to an unfortunate mistake the parameters of the potential in the original papers appeared incorrectly. The numbers are corrected in subsequent Errata,^{17b,18b} and are also listed here in Table 1. The long-range part of the electrostatic interaction has been treated by the Ewald method¹⁵ in the MD calculations and by the reaction field correction method²³ in the MC simulations. The geometry of the rigid formic acid molecules is taken from ref 17. We note that similarly to earlier works,^{17,18} we considered only the *cis* conformer of formic acid being 20–25 kJ/mol more stable in free energy at 298.15 K than the *trans*-formic acid.^{2,22} The high energy barrier of approximately 60 kJ/mol also prevents the *cis*–*trans* interconversion.²²

We also note that extensions of the simple electrostatic plus Lennard-Jones type potentials are also available in the literature. Explicit inclusion of many-body effects is possible via the application of molecular polarizabilities as illustrated recently on the examples of acetone, formaldehyde, and formic acid.²⁴ Other types of modifications of the simple van der Waals and charge interaction potential for formic acid were also proposed by incorporating charge fluxes and atomic dipoles in the electrostatic model.²⁵ In many cases carefully optimized all-site effective pair potentials can be sufficient. Since our earlier developed pairwise, additive, effective potential successfully reproduces both thermodynamic and structural properties of the liquid phase, we think that the model is a reliable and economic choice for the present purposes. Nevertheless, one always has to be aware of the limitations of the two-body approach. This point will be also emphasized in the following discussion.

Results and Discussion

Molecular Dynamics Simulations. Dynamic and Spectroscopic Properties. Molecular dynamics simulations were performed on the microcanonical ensemble with 500 formic acid molecules in a cubic simulation box. We applied the quaternion procedure to ensure the rigidity of the individual molecules in our MD scheme.²⁶ The classical equations of motion were integrated by the Verlet algorithm²⁷ using a 1 fs time step. After an initial 20 ps equilibration period, we carried out a 50 ps long preequilibrium run followed by a 150 ps long equilibrium trajectory. The average temperature during the equilibrium run was 301.5 K.

The first dynamic property we focus on is the self-diffusion constant. Two schemes are employed to calculate *D* in the literature.¹⁵ The Einstein relation makes use of the long-time limit of the mean-square displacement of the sites of the molecules. This approximation predicts 1.46×10^{-5} cm²/s, about 40% higher than the experimental 1.04×10^{-5} cm²/s.¹² The self-diffusion coefficient may also be calculated from the integral of the velocity autocorrelation function of the center-of-mass of the individual molecules. The velocity autocorrelation function is shown in Figure 1. We found that the *integral* of the autocorrelation function as a function of time (not shown) exhibits strong fluctuations after a very fast increase (in the first 200 fs) and a more or less monotonic decrease up to 10 ps. After 10 ps the integral function appears to contain significant contribution from statistical noise. An exponential fit to the decreasing part of the integral function up to 10 ps results in 1.30×10^{-5} cm²/s in the long-time limit for the self-diffusion constant with somewhat better agreement with the experimental value than that obtained from the Einstein relation.

The velocity autocorrelation functions are intimately connected to the various modes of molecular motions. More precisely, the Fourier transforms of the center-of-mass velocity autocorrelation function and of the angular velocity autocorrelation functions around the three principal axes provide the spectral densities for the hindered translational and rotational motions, respectively. The computed spectral densities for the translational motions are shown in Figure 1 with a peak in the spectrum at 50 cm⁻¹ and a pronounced shoulder at around 200 cm⁻¹. To understand the origin of the two bands deeper, we separated the center-of-mass velocity into two contributions, one in the molecular plane (xy plane), the other perpendicular to the same plane (z direction). The Fourier transforms of the corresponding components clearly indicate (see Figure 1) that the higher wavenumber shoulder originates predominantly from the in-plane motions, while both components contribute sig-

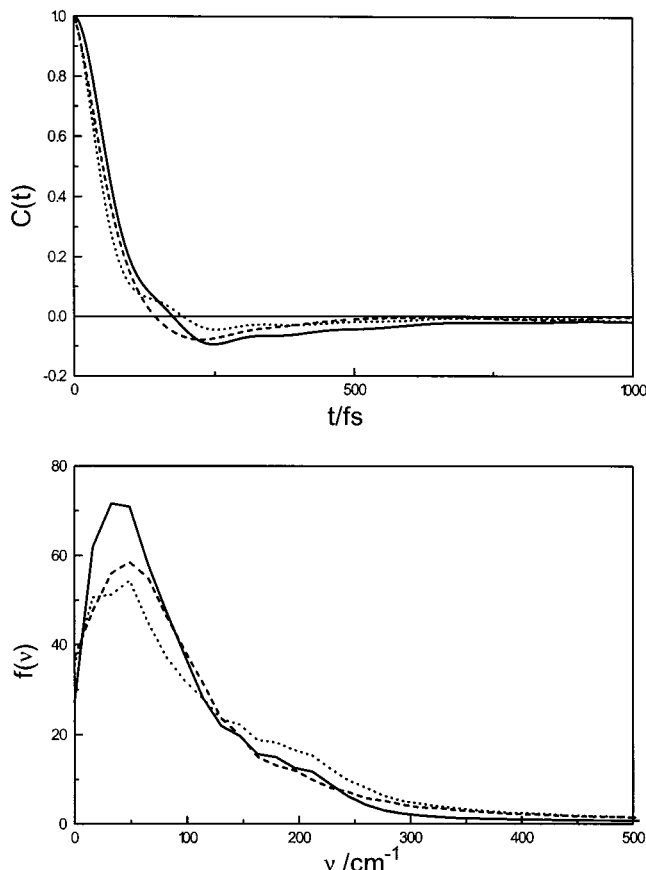


Figure 1. Translational velocity autocorrelation functions (upper) and the corresponding spectral densities (lower) for liquid formic acid. Spectral densities in arbitrary units. Solid line: total autocorrelation function and spectral density; dashed lines: the component perpendicular to the molecular plane; dotted lines: the planar component.

nificantly to the less hindered peak at 50 cm^{-1} . Figure 2 shows the three angular velocity autocorrelation functions and the corresponding rotational spectral densities. The calculation of the rotational spectral densities is based on the treatment of Heinzinger et al. on the spectroscopic properties of substituted water.²⁸ Vibrations around the x and y axes (in the principal axis coordinate system) are quasidegenerate with maxima located at 200 cm^{-1} , while the peak of the in-plane libration (around the z axis) shifts toward lower wavenumbers (approximately 100 cm^{-1}).

To facilitate the discussion of the spectra of liquid formic acid, we collected the harmonic intermolecular vibrational frequencies for four different minima of the formic acid dimer potential surface calculated at MP2/6-31G(d) level and the gas phase experimental frequencies of the most stable dimer, **II**, in Table 2 (for the numbering of the dimers see Figure 3).^{2,22,29} Although the experimentally observed Raman bands can be attributed to the coalescence of the manifold of peaks arising from various highly collective and anharmonic molecular modes, comparison of the gas phase dimer intermolecular frequencies to the calculated spectral densities and the experimental spectrum turns out to be illustrative. First of all, it is noticeable that weakly hydrogen-bonded dimers (for example, **VII** and **VIII**) do not possess bands at the higher wavenumber region of 200 cm^{-1} . This important feature of the density spectra can be correlated reasonably with the normal modes of the two most stable dimers, **II** and **III**. Most characteristically, the in-plane symmetric stretch of the hydrogen-bonding system of **II** (ν_4) appears as a translational mode and is likely responsible for the 200 cm^{-1}

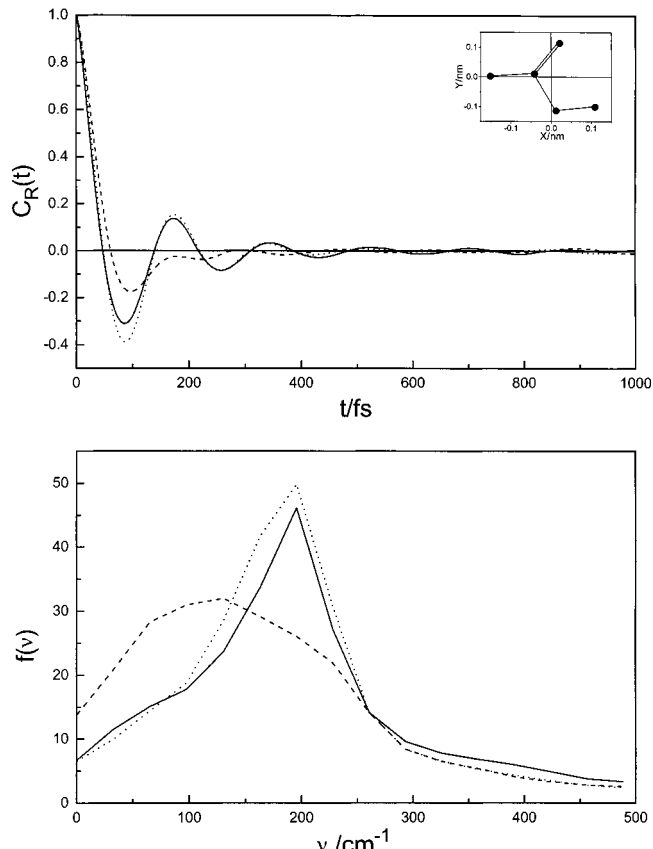


Figure 2. Rotational velocity autocorrelation functions (upper) and the corresponding spectral densities (lower) for liquid formic acid. The inset shows the orientation and the three principal axes of the formic acid molecule. Spectral densities in arbitrary units. Solid line: rotation around the x axis; dotted line: rotation around the y axis; dashed line: rotation around the z axis.

TABLE 2: Calculated (Harmonic) Vibrational Frequencies (in cm^{-1}) for Dimers **II, **III**, **VII**, and **VIII** at MP2/6-31G(d) Level^{2,22} (Experimental Frequencies Are in Parentheses)^a**

vibrations	II	III	VII	VIII
ν_1	72 (68) A_u	63	22	36
ν_2	168 (137) A_g	121	71	84
ν_3	176 (163) A_u	123	75	94
ν_4	206 (190) A_g	148	77	103
ν_5	270 (230) B_g	196	79	108
ν_6	265 (248) B_u	208	87	110

^a Reference 29 and references therein.

shoulder in the translational spectrum. The out-of-plane rotation around the y axis (ν_5), the in-plane antisymmetric stretch (ν_6) for **II**, and the in-plane libration of **III** (ν_6) also contribute in the same region, although at slightly higher frequencies. These frequencies correlate qualitatively with the rotational spectral densities for the y and z axes; the former function has its maximum around 200 cm^{-1} and the latter has also significant contribution here (see Figure 2). On the other hand, we have not been able to identify such dimer intermolecular modes which could be responsible for the rotational band around the x axis. This finding might imply that, in addition to the dimer intermolecular modes examined above, additional, relatively stiff intermolecular modes should be present in the liquid phase. A more quantitative assignment is obviously hampered by the harmonic approximations involved in the calculations, the lack of order of the liquid state, and the statistical distributions of the intermolecular interactions. Since the simulated spectra are very sensitive to the shape of the potential energy surface, the

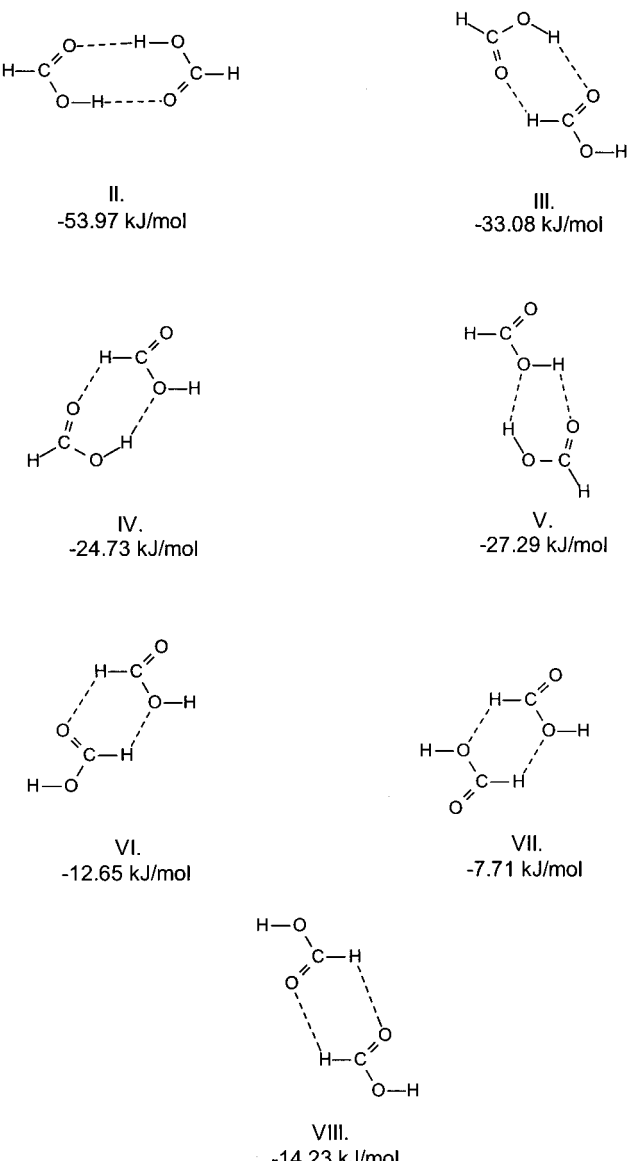


Figure 3. Structures of seven minima located on the ab initio potential surface with the stabilization energies of the present parameter set.^{2,17} The numbering follows that in refs 2, 17, and 18. Species **I** is the *cis*-formic acid monomer.

use of an effective pairwise potential presents another serious obstacle to a more precise comparison. Experimentally, the wide distribution of interactions manifests in broad spectral bands. Accordingly, an earlier Raman spectroscopic work¹⁰ observed two broad low-frequency bands centered approximately at 80 and 200 cm⁻¹. A very recent Raman spectroscopic study¹¹ performed in the 80–4000 cm⁻¹ range finds one broad band in the low-frequency regime at around 200 cm⁻¹. Despite the present approximations (use of an effective pairwise potential and the harmonic approximation) we can conclude that the general features of the calculated spectral densities agree reasonably well with the experimental liquid state Raman spectrum.

The velocity autocorrelation functions are closely related to the relaxation phenomena of the liquids through the molecular level reorientational motions. In general, the reorientational motions are characterized in terms of the autocorrelation functions of the Legendre polynomials.^{30,31}

$$C_l(t) = \langle P_l(\cos \theta(0)) P_l(\cos \theta(t)) \rangle \quad (1)$$

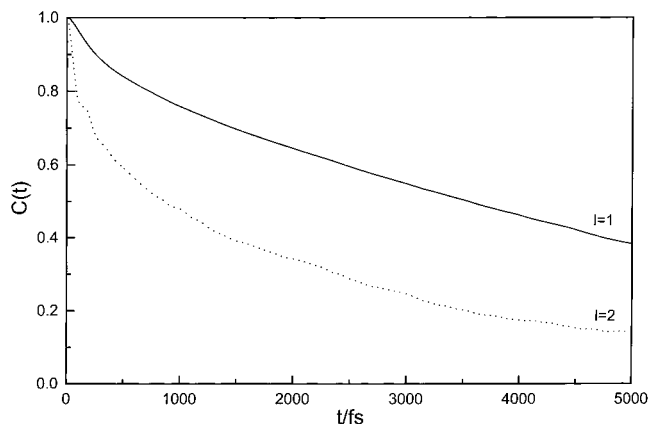


Figure 4. First two members of the $C_l(t)$ series of the autocorrelation functions of the Legendre polynomials for the dipole direction ($C_1(t)$) and for the O–H bond direction ($C_2(t)$).

In eq 1 $\theta(t)$ is the angle of the rotation of a molecule-fixed vector. The first two members of the series ($l = 1, 2$) can be easily related to the experimentally measured relaxation time scales of the liquids. Figure 4 shows $C_1(t)$ and $C_2(t)$ for the molecular dipole and OH bond direction, respectively. Since $C_1(t)$ is proportional to the dipole autocorrelation function, single-molecule correlation time (τ_1) can be deduced from the Debye-like long-time exponential decay of this correlation function.³² The fitted decay time turns out to be 6 ps, while the integral correlation time becomes about 5 ps. The direct comparison of the calculated single-particle correlation time and the experimentally obtainable macroscopic dielectric relaxation time (τ_D) is quite a difficult issue even in the case of a simple exponential decay.³³ The Cole–Cole plots for liquid formic acid¹⁴ reveal, however, that there exist at least two dielectric decay domains with 2.08 and 40 GHz critical frequencies at 298 K, corresponding to macroscopic relaxation times of 74 and 4 ps, respectively. For the simplest comparison, one can utilize the following relation of Powles for the macroscopic and the microscopic relaxation times of the i th exponential decay:³³

$$\frac{\tau_{D,i}}{\tau_{1,i}} = \frac{3\epsilon_{0,i}}{2\epsilon_{0,i} + \epsilon_{\infty,i}} \quad (2)$$

Taking the corresponding experimental data (the frequency dependent dielectric constants and the relaxation time) for the second domain,¹⁴ we can approximate the “experimental” single-particle correlation time as 3.1 ps in modest agreement with the simulated data (note that we observe only the faster relaxation from our molecular dynamics simulations).

Beyond its significance in neat liquids, the dipole autocorrelation function has a prominent role in the theory of solvation dynamics of monatomic solutes which undergo step-function change in the charge. The function $\{C_1(t)\}^\alpha$ can successfully reproduce the autocorrelation function of the equilibrium fluctuations of the solvation energy,^{34,35} which, in turn, coincides in the linear response approximation with the nonequilibrium response function of the solvation energy during the solvation process. The translation factor between individual rotational motions and solvation response, α , is basically equivalent with the dipole density multiplied by a screening by the solvent polarity:³⁵

$$\alpha = \left\{ \frac{4\pi\rho\mu^2}{3k_B T} \right\} \left(1 - \frac{1}{\epsilon} \right)^{-1} \quad (3)$$

where ρ is the number density of the solvent, μ is the dipole moment, and ϵ is the static dielectric constant. In general, large α implies that the solvation energy may relax significantly for a slight molecular rotation in the liquid, while the dipole autocorrelation function is only hardly influenced. The resulting $\alpha = 24$ value for neat formic acid is similar to those for water and acetonitrile ($\alpha = 19$ and 20, respectively),³⁵ and significantly higher than for methanol ($\alpha = 8$).³⁴ The factor α also relates single-particle motions with the solvation response by providing the connection between the free rotational motion of the solvent molecules and the solvation frequency ($\omega_s^2 = \alpha \langle \omega_1^2 \rangle$), the solvation frequency (ω_s) defined as the curvature of the equilibrium response function at $t = 0$. The free rotational frequency for the formic acid molecule can be approximated as the average of the free rotational frequencies ($\omega_1 = (k_B T / I)^{1/2}$) for the x and z axes (see the inset in Figure 2 for the molecular orientation and note that y approximately coincides with the dipole direction). These simple relations result in an estimate of $\omega_1 = 2.3 \text{ ps}^{-1}$ for the average free rotational frequency and $\omega_s = 11.3 \text{ ps}^{-1}$ for the solvation frequency. The inertial regime of the (linear) solvation response of liquid formic acid has, thus, qualitatively similar frequency as for acetonitrile ($\omega_s = 14.0 \text{ ps}^{-1}$), but is much slower than for water ($\omega_s = 100 \text{ ps}^{-1}$).³⁵ The similar α and ω_s values indicate that the equilibrium response function for the solvation of a monatomic solute in formic acid can be expected to have similar behavior to that in acetonitrile.

The correlation time of the second member of the series from eq 1 is closely related to the longitudinal or spin-lattice relaxation time (T_1) obtainable from NMR measurements. The assumption of isotropic rotation in the “extreme narrowing” limit leads to a linear relation between the spin-lattice relaxation rate and the molecular reorientational correlation time, τ_2 .^{12,36,37}

$$1/T_1 = \frac{3}{2}\pi^2\Theta^2\tau_2 \quad (4)$$

The proportionality constant in eq 4 contains the square of the quadrupole coupling constant for the deuteron, Θ . The experimentally measured relaxation rate ($1/T_1$) determined by Kratochwill and Hertz¹² for deuterated formic acid (HCOOD) is 4 s^{-1} . They assumed a value of 200 kHz for Θ in the neat liquid, which is 20% higher than in the solid phase, and obtained 6.5 ps for τ_2 .¹² Employing the experimental value of 272 kHz by Ruben and Kukolich¹³ with the same experimental relaxation rate, one receives 3.65 ps for the molecular reorientational time. Our computed relaxation time from the slope of the linear part of the logarithm of $C_2(t)$, 3.8 ps, is in excellent agreement with the latter experimental figure. Thus, although the experimentally deduced τ_2 values may be put in a fairly wide distribution, the present simulations produce a promising estimate for the molecular relaxation time.

Hydrogen-Bonding Dynamics. We have already referred (as, for example, in eq 3) to the role the intermolecular interactions play in influencing the molecular reorientational motions. The role of the hydrogen bonds, as the strongest of this type of interactions, is fundamental. In our previous work, we considered the statistical properties of the hydrogen-bonding structure of neat liquid formic acid.¹⁸ The MD investigations can provide supplementary information on the hydrogen-bonding dynamics. In particular, we should like to examine the lifetimes of the individual hydrogen bonds possible in liquid formic acid, and as a further step, the various hydrogen-bonded dimers. The hydrogen-bonding dynamics also have essential implications for the aggregation of the molecules.

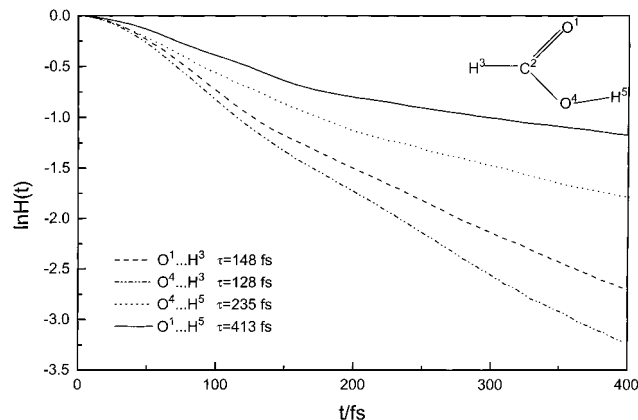


Figure 5. Decay functions for the four different types of hydrogen-bonding interactions in liquid formic acid. The inset shows the numbering of the atoms of the formic acid molecule.

In the first step, we calculate the fraction of the hydrogen bonds ($H(t)$) that remain unbroken after a time t employing the method applied for methanol clusters by Haughney et al.³¹ The procedure involves counting the number of bonds ($N(t_n)$) that break precisely after the n th time step:

$$H(t_m) = \sum_{n=m}^{\infty} N(t_{n+1}) / \sum_{n=1}^{\infty} N(t_n) \quad (5)$$

The mean lifetime of the hydrogen bond can then be defined as follows:

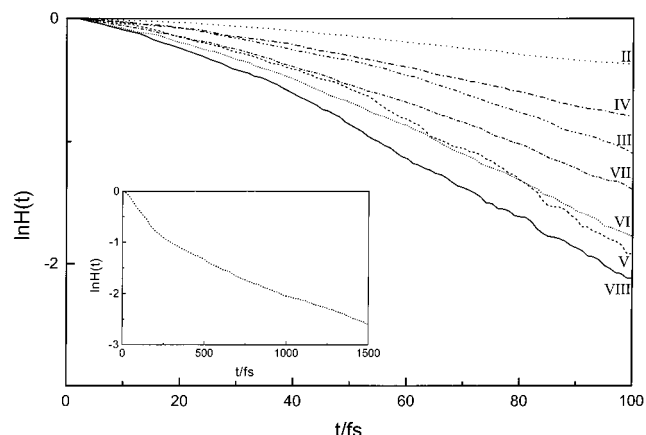
$$\tau = \sum_{n=0}^{\infty} \frac{\Delta t}{2} [H(t_n) + H(t_{n+1})] \quad (6)$$

As the initial condition we know that $H(0) = 1$ and Δt is the time step of the simulation. Following the lines of our previous work,^{2,17,18} we can distinguish four types of H-bonds, two different O-H \cdots O and two C-H \cdots O interactions. The definition of these hydrogen bonds requires the $r_{(O)H\cdots O}$ and $r_{(C)H\cdots O}$ distances be shorter than 2.5 Å and the $\alpha_{O-H\cdots O}$ and $\alpha_{C-H\cdots O}$ angles be larger than 130°. We found that an average formic acid molecule participates in 1.85 O-H \cdots O hydrogen bonds, and 2.78 H-bonds including the C-H \cdots O interactions. These numbers are consistent with earlier observation for the hydrogen-bond structure of liquid formic acid.¹⁸ The resulting decay functions are shown in Figure 5. It is evident that the weaker C-H \cdots O bonds break faster, and, consequently, live shorter. The calculated lifetimes are correspondingly 400 fs for the strongest O-H \cdots O hydrogen bonds and approximately 150 fs for the C-H \cdots O hydrogen bonds.

One may also want to compare the dominant interactions in the gas and solid phases to those in the liquid by examining whether there exist molecule pairs (dimers) in the liquid phase with two simultaneous hydrogen bonds within the pairs. The classification of these pairs with double hydrogen bonds corresponds to those dimers which are local minima on the gas phase dimer potential surface (see Figure 3 and ref 2). In the gas phase, **II** is the dominant dimer, while the crystalline chains are formed from dimeric units similar to **III**. For the definition of dimeric interactions with two H-bonds we found that the distance criteria applied for the two interactions simultaneously is sufficient to sample the relevant species. Furthermore, since in the optimized gas-phase dimers all hydrogen–oxygen distance of the C-H \cdots O interactions is about 2.5–2.6 Å,² we allowed for a less stringent H-bonding distance for the C-H \cdots O

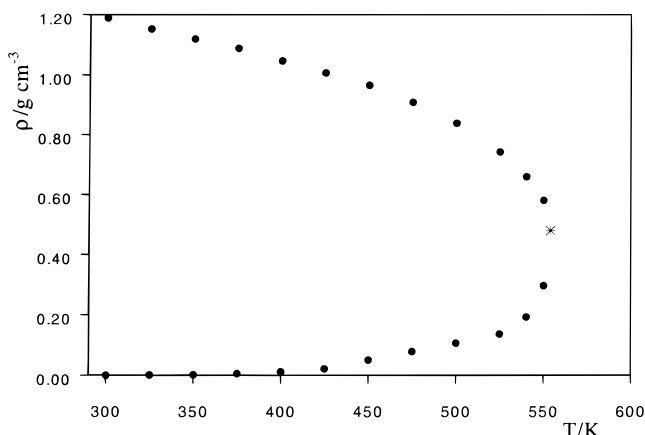
TABLE 3: Relative Fractions (%) and Average Lifetimes (fs) of Various Dimers with Two Hydrogen Bonds between the Two Connected Monomeric Units

	relative dimer fraction (%)	average lifetime (fs)		relative dimer fraction (%)	average lifetime (fs)
II	63.5	458	VI	4.4	62
III	9.0	101	VII	8.2	76
IV	10.4	130	VIII	2.9	51
V	1.6	62			

**Figure 6.** Decay functions for dimer interactions with two hydrogen bonds. For numbering see Figure 3. The inset shows a longer time scale decay for dimer **II**.

hydrogen bonds ($r_{(C)H\cdots O} < 2.7 \text{ \AA}$). The relative populations of the dimers with two hydrogen bonds are listed in Table 3. Due to the inherent arbitrariness in defining individual hydrogen bonds and subsequently doubly hydrogen-bonded dimers, the absolute numbers should be carefully interpreted. Nevertheless, a few qualitative observations are in order. First of all, more than 60% of the double hydrogen-bonding interactions are of type **II**, which, in turn, are formed by only 7% of the formic acid molecules.¹⁸ The weights of the other dimers increase substantially relative to the gas phase. The shift in the relative populations of the various double H-bonded species is the result of the fine interplay between both energetic and entropic factors determining the structure and dynamics of the condensed phases. As an example, the 520:1 ratio for **II** and **III** at 298 K calculated for the gas phase² decreases to only 7:1 in the liquid phase. This particular shift of the relative weight of **III** shows that the dimeric interactions, dominant in the solid phase, are already present in liquid formic acid (approximately 1% of the molecules). The importance of the various double hydrogen-bonded dimers is also reflected in the decay functions (Figure 6) and the average lifetimes collected in Table 3. The lifetimes of the doubly H-bonded species correlate strongly with the lifetimes of the individual hydrogen bonds (see Figures 5 and 6).

Vapor–Liquid Equilibrium. The vapor–liquid coexistence curve of our formic acid model was calculated from a set of simulations using the Gibbs ensemble Monte Carlo technique.²⁰ Simulations of this type treat the liquid and the vapor systems simultaneously, and establish thermodynamic equilibrium by letting the two systems to exchange both volume and molecules. The key to the efficiency of the method is the fact that the two systems have no actual interface. Since the method tends to break down at lower temperatures (i.e., at higher densities), the systems at lower temperature were treated by the cavity-biased variant of the method,²¹ in which analogously to the grand canonical ensemble cavity biased method,³⁸ insertions are only

**Figure 7.** Vapor–liquid equilibrium densities of formic acid as a function of the temperature, as resulted from Gibbs ensemble Monte Carlo simulations with the present model. The asterisk is the estimated critical point of the model.

attempted into preexisting cavities and the acceptance of such attempted changes is modified to correct for this bias.

Simulations were performed at 12 different temperatures, namely at 300, 325, 350, 375, 400, 425, 450, 475, 500, 525, 540, and 550 K. The two cubic simulation boxes contained 601 formic acid molecules altogether. Molecule and volume exchange steps were attempted after every pair of displacement steps and after every 600 displacement attempt pairs, respectively. Cavity biasing has only been used at the temperatures below 525 K when a molecule was attempted to transfer from the dilute (vapor) to the dense (liquid) phase. In such cases the insertion of the molecule was attempted into cavities of radius fluctuating around 3.3 Å. The maximum translation and rotation of a particle in the displacement steps were 0.3 Å and 15°, respectively. The maximum change of the box volume in one step was 400 Å³. The systems were equilibrated by about 50–75 million pairs of particle displacement steps, whereas in the production phase 15 million particle displacement pairs were attempted.

The calculated densities of the coexisting vapor and liquid phases are shown in Figure 7 as a function of the temperature. The critical temperature and density of the model were estimated to be $T_c = 554 \text{ K}$ and $\rho_c = 0.48 \text{ g/cm}^3$ by fitting a sixth-order polynomial to the density values at the five highest temperatures. Similar values were obtained when a fifth-order polynomial was fitted to the points above 500 K. Unfortunately, we can only compare the simulated critical temperature with the experimental value of $T_c^{\text{exp}} = 588 \text{ K}$,⁸ since, to our knowledge, the experimental liquid–vapor coexistence curve, as well as the critical density of liquid formic acid, has not been reported yet. Nevertheless, the two facts that (i) the model is able to reproduce the experimental critical temperature well, within about 5%, and (ii) it reproduces the experimental density very well, within about 1% at 298 K,¹⁷ suggest that the curvature of this phase diagram is probably reproduced rather accurately by the model. The experimental determination of the vapor–liquid equilibrium properties of formic acid would provide a very important and useful test of the present potential model. A possible good agreement with the present results, which can be expected from the good reproduction of the critical temperature, could verify that the model can indeed describe the thermodynamic properties of formic acid well over a very broad range of thermodynamic states.

Excess Free Energy. The excess free energy of liquid formic acid at 298 K was calculated by the thermodynamic integration

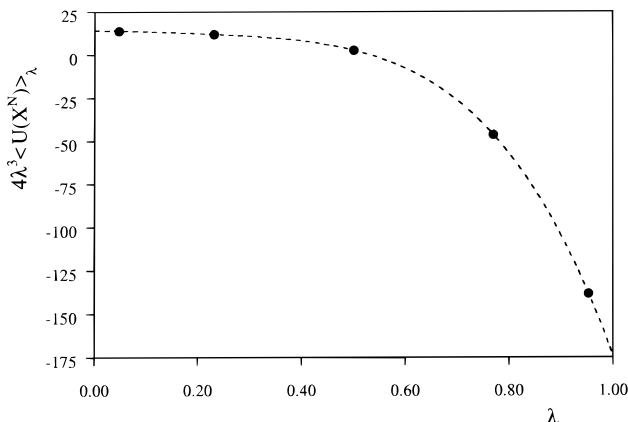


Figure 8. Integrands of the thermodynamic integration (see eq 8) of the excess free energy calculation at 298 K at the coupling parameter values of the Gaussian quadrature used (dots). The dashed curve is the approximating fourth-order polynomial fitted to the values at the quadrature points.

method.³⁹ The underlying ideal gas and the liquid was connected in the configuration space by the following path defined by the coupling parameter λ :

$$E(X^N, \lambda) = \lambda^4 U(X^N) \quad (7)$$

Previous examples for such calculations, including an enhanced path for the definition of $E(X^N, \lambda)$, can be found elsewhere.⁴⁰ The excess free energy A' can be then obtained from the relation

$$A' = \int_0^1 4\lambda^3 \langle U(X^N) \rangle_\lambda d\lambda \quad (8)$$

As has been discussed elsewhere,³⁹ in three dimensions for a potential energy with an r^{-12} repulsion term the exponent 4 on λ in eq 7 eliminates the singularity at the $\lambda = 0$ end of the integral of eq 8. The symbol $\langle \dots \rangle_\lambda$ indicates the Boltzmann average of the quantity enclosed, being $E(X^N, \lambda)$ instead of $U(X^N)$ in the Boltzmann factor. From the technical point of view, this average is equivalent to the usual Boltzmann average at the temperature $T^* = T/\lambda^4$. The integral was evaluated numerically, using a five-point Gaussian quadrature. The integrand at each quadrature point, shown in Figure 8 as a function of the coupling parameter, was calculated from (N, V, T) ensemble Monte Carlo simulations of 512 molecules, performed at the corresponding T^* temperature. By performing the integration of eq 8, the excess free energy value of $A' = -22.07$ kJ/mol was obtained. A' is related to the excess entropy S' and excess chemical potential μ' through the relations:

$$S' = \frac{(A' - \langle U \rangle)}{T} \quad (9)$$

$$\mu' = A' + pV \frac{N_A}{N} - RT \quad (10)$$

From these equations the excess entropy and excess chemical potential of the model at 298 K resulted in 58.36 J/(mol·K) and -24.54 kJ/mol, respectively.

Conclusions

The present work, a detailed, classical liquid simulation study using molecular dynamics and Monte Carlo techniques, completes a series of earlier investigations on the energetics, structure, and thermodynamics of formic acid.^{2,17,18} Here, we

have investigated several dynamic, spectroscopic, and further thermodynamic aspects of the neat liquid. Although the agreement is not quantitative between some calculated and measured properties (i.e., the diffusion constant), the emerging picture provides a valuable insight into the molecular contributions underlying various, interesting properties of the liquid phase. The qualitative assignment of the broad bands of the low-frequency Raman spectrum based on the calculation of the translational and rotational spectral densities is an illustrative example. The simulated molecular reorientational times also correlate well with the relaxation times from dielectric measurements and NMR spectroscopy. A simple relation between single-particle rotational motions and solvation response³⁵ makes it possible to predict solvation dynamics of a monatomic solute in neat liquid formic acid from the free rotational times of formic acid molecules and the dipole autocorrelation function. We predict the solvation dynamics of liquid formic acid in the linear response approximation to be similar to that of acetonitrile. The complex hydrogen-bonding structure of liquid formic acid and its dynamics have been investigated in terms of the lifetimes of the various types of hydrogen bonds. The average lifetime of the stronger O—H \cdots O hydrogen bonds appears to be about 4 times longer than that for the C—H \cdots O interactions. A similar analysis for the double hydrogen-bonded dimers revealed that the relative weight of the dimers characteristic of the crystalline phase is significantly higher in the liquid phase than calculated for the gas phase.² As a straightforward extension of the calculations for the liquid phase, thermodynamic calculations were also performed for the vapor–liquid equilibrium. The results (vapor–liquid coexistence curve, critical temperature), on the one hand, further verify the applicability of the present formic acid model over a broad range of thermodynamic states. On the other hand, we could also predict experimentally not yet available thermodynamic excess quantities as the excess free energy, excess entropy, and the excess chemical potential at 298 K.

Acknowledgment. L.T. gratefully acknowledges the financial support from the National Research Fund of Hungary (OTKA) under Contract No. F031996. P.J. is an Eötvös Fellow of the Hungarian Ministry of Education, which is gratefully appreciated.

References and Notes

- Gu, Y.; Kar, T.; Scheiner, S. *J. Am. Chem. Soc.* **1999**, *121*, 9411.
- Turi, L. *J. Phys. Chem.* **1996**, *100*, 11285.
- Kwei, G.; Curl, R. *J. Chem. Phys.* **1960**, *32*, 1592.
- (a) Nahringbauer, I. *Acta Crystallogr.* **1978**, *B34*, 315. (b) Albinati, A.; Rouse, K. D.; Thomas, M. W. *Acta Crystallogr.* **1978**, *B34*, 2188.
- Swan, I. G. In *Hydrogen-Bonded Liquids*; Dore, J. C., Teixeira, J., Eds.; NATO ASI Series C, Kluwer Academic: Dordrecht, The Netherlands, 1991; p 139.
- Nasr, S.; Bellissent-Funel, M.-C.; Cortès, R. *J. Chem. Phys.* **1999**, *110*, 10945.
- CRC Handbook of Chemistry and Physics*, 75th ed.; Lide, D. R., Frederiksen, H. P. R., Eds.; CRC Press: Boca Raton, FL, 1994–95.
- Lide, D. R. *Handbook of Organic Solvents*; CRC Press: Boca Raton, FL, 1995; p 248.
- Chapman, D. *J. Chem. Soc.* **1956**, 225.
- Blumenfeld, S. M.; Fast, H. *Spectrochim. Acta* **1968**, *24A*, 1449.
- Bartholomew, R. J.; Irish, D. E. *J. Raman Spectrosc.* **1999**, *30*, 325.
- Kratochwill, A.; Hertz, H. G. *J. Chim. Phys.* **1977**, *74*, 814.
- Ruben, D. J.; Kukolich, S. G. *J. Chem. Phys.* **1974**, *60*, 100.
- Constant, E.; Lebrun, A. *J. Chim. Phys.* **1964**, *61*, 163.
- Three comprehensive works from the field: Allen, M. P.; Tildesley, D. J. *Computer Simulation of Liquids*; Clarendon: Oxford, UK, 1987. Ciccotti, G., Frenkel, D., McDonald, I. R., Eds. *Simulation of Liquids and Solids*; Elsevier: Amsterdam, 1987. Frenkel, D.; Smit, B. *Understanding Molecular Simulation*; Academic Press: San Diego, CA, 1996.

(16) Jedlovszky, P.; Bakó, I.; Pálinkás, G.; Dore, J. C. *Mol. Phys.* **1995**, 86, 87.

(17) (a) Jedlovszky, P.; Turi, L. *J. Phys. Chem. A* **1997**, 101, 2662. (b) Erratum: *J. Phys. Chem. A* **1999**, 103, 3796.

(18) (a) Jedlovszky, P.; Turi, L. *J. Phys. Chem. B* **1997**, 101, 5429. (b) Erratum: *J. Phys. Chem. B* **1999**, 103, 3510.

(19) Car, R.; Parrinello, M. *Phys. Rev. Lett.* **1985**, 55, 2471.

(20) Panagiotopoulos, A. Z. *Mol. Phys.* **1987**, 61, 813.

(21) Mezei, M. *Mol. Simul.* **1992**, 9, 257.

(22) Turi, L. Unpublished results.

(23) Barker, J. A.; Watts, R. O. *Mol. Phys.* **1973**, 26, 789. Neumann, M. *J. Chem. Phys.* **1985**, 82, 5663.

(24) Hermida-Ramón, J. M.; Ríos, M. A. *J. Phys. Chem. A* **1998**, 102, 2594. Hermida-Ramón, J. M.; Ríos, M. A. *J. Phys. Chem. A* **1998**, 102, 10818. Hermida-Ramón, J. M.; Ríos, M. A. *Chem. Phys.* **1999**, 250, 150.

(25) Qian, W.; Krimm, S. *J. Phys. Chem. A* **1997**, 101, 5825. Qian, W.; Krimm, S. *J. Phys. Chem. A* **1998**, 102, 659.

(26) Fincham, D.; Smith, W. CCP5 Program Library.

(27) Verlet, L. *Phys. Rev.* **1967**, 159, 98.

(28) Lu, T.; Tóth, G.; Heinzinger, K. *J. Phys. Chem.* **1996**, 100, 1336.

(29) Chang, Y.-T.; Yamaguchi, Y.; Miller, W. H.; Schaefer, H. F., III. *J. Am. Chem. Soc.* **1987**, 109, 7245.

(30) Rahman, A.; Stillinger, F. H. *J. Chem. Phys.* **1971**, 55, 3336.

(31) Haughney, M.; Ferrario, M.; McDonald, I. R. *J. Phys. Chem.* **1987**, 91, 4934.

(32) McQuarrie, D. A. *Statistical mechanics*; Harper & Row: New York, 1976.

(33) Powles, J. G. *J. Chem. Phys.* **1953**, 21, 633.

(34) Stratt, R. M.; Maroncelli, M. *J. Phys. Chem.* **1996**, 100, 12981.

(35) Maroncelli, M.; Kumar, V. P.; Papazyan, A. *J. Phys. Chem.* **1993**, 97, 13.

(36) Abragam, A. *Principles of Nuclear Magnetism*; Clarendon, Oxford, UK, 1961.

(37) Versmold, H. *Ber. Bunsen-Ges. Phys. Chem.* **1980**, 84, 168.

(38) Mezei, M. *Mol. Phys.* **1980**, 40, 901; **1987**, 61, 565; Erratum: **1989**, 67, 1207.

(39) Mezei, M.; Beveridge, D. L. *Ann. Acad. Sci. N.Y.* **1986**, 482, 1.

(40) Mezei, M. *J. Comput. Chem.* **1992**, 13, 651.